SAND2009-2935C

Validation Assessment for Modeling the Thermal Response of Components Embedded in Removable Epoxy Foam – Numerical Modeling and Comparison*

R. E. Hogan, K. J. Dowding, M. L. Hobbs, K. L. Erickson, and S. M. Trujillo

Engineering Sciences Center
Sandia National Laboratories
Albuquerque, New Mexico, USA

ABSTRACT

A series of validation experiments and analyses has been performed to assess the predictive capability of thermal response models for objects embedded in Removable Epoxy Foam (REF). Data, model predictions, and quantified uncertainties were employed in a validation process to assess model predictive capability. Validation quality data were obtained with at least two replicate experiments for each combination of hold temperature and orientation. A numerical model for predicting the heat transfer through the decomposing foam to the embedded component is presented in detail. A quantitative comparison of the model predictions and experimental data is presented. Uncertainty and parameter sensitivity analyses were used to assess the solution uncertainty and to identify the dominant model parameters.

INTRODUCTION

A rigorous validation assessment to quantify the accuracy of a numerical model for safety applications in abnormal thermal environments is presented. This validation assessment considers the thermal response of an object embedded in removable epoxy foam (REF). The experimental aspects of this validation assessment are presented in detail in a complementary paper by Dowding et al. (2009).

In the work reported by Dowding et al. (2009), the details of the experimental component of this project were presented. The experimental data were analyzed and studied to quantify the dependence on the unit configuration (hold temperature/orientation) using time-based metrics, which have relevance for the intended application. Repeatability of the experiments and variability from unit to unit were also addressed. As part of assessing the model, experimental data are assessed independently. The experimental assessment quantifies and studies the repeatability of the experiment, the dependence of the experiments on configuration, and the experimental variability.

In this paper, we present the details of the quantitative comparison of model predictions and the experimental data. Differences between the model predictions and experimental measurement were quantitatively studied using time-based metrics. The magnitude and dependence on configuration of the differences were quantified. An assessment of the model's accuracy was inferred from this quantification.

The analysis addressed the effect of uncertainty in the model parameters and boundary conditions used to model the experimental setup. The estimated uncertainty in the model predictions was used in the comparison with the experimental measurements, with experimental uncertainty and variability also estimated, to gauge the difference between measurements and model predictions. Additionally, the analysis of model uncertainty identified the model parameters which had the largest impact on the uncertainty estimates.

An overview of the complementary experiments is first presented. The mathematical models are next described, followed by detailed comparisons of the experimental data and model predictions. Quantification of the comparison of model predictions and measured data include the effects of uncertainty in both the experiments and the numerical model.

EXPERIMENTAL SETUP

The experimental program providing data for the validation is described in Dowding et al. (2009) and Erickson et al. (2009). An overview of the experimental test units and the thermocouple locations are summarized here for convenience. The details of the experimental apparatus and test operation are provided in the companion paper by Dowding et al. (2009).

Instrumentation

The details of the experimental instrumentation are described because the thermocouple data are used to control the heating, provide boundary conditions, and in comparisons with the model predictions. The foam-in-can (FIC) assembly was instrumented with 24 thermocouples (TCs) as shown in Figure 1. The end plates have four thermocouples (1-4 and 13-16) equally spaced around the circumference of the plate, extending 2.54 cm (1 inch) from the outer edge on the "top" (1-4) and 1.11 cm (0.438 inches) on the "bottom" (13-16) location and approximately halfway through the plate thickness. A bank of four thermocouples (5-8 and 9-12) was equally spaced along the length, located on opposite sides of the cylindrical assembly. The embedded component was instrumented with three thermocouples just below the surface (17, 18, and 20) on the solid end. A single thermocouple was on the back surface of the solid end (19) and four thermocouples (21-24) were located along the walls of the cavity machined in the component.

An experimental run consisted of heating the "heated plate" with radiant heat lamps. The temperature

*Sandia is a multiprogram laboratory operated by Sandia Corporation, a Lockheed Martin Company, for the United States Department of Energy's National Nuclear Security Administration under contract DE-AC04-94AL85000.

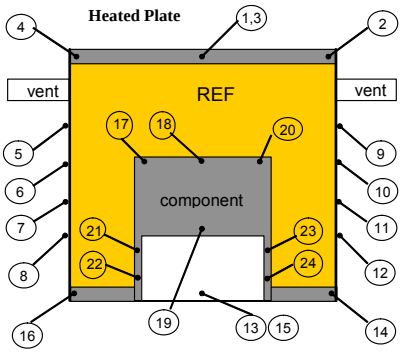

Figure 1. Thermocouple locations on test can

of the heated plate (TCs 1-4) was increased at a rate of 200 °C/min up to a specified hold temperature of either 750 °C or 900 °C Then, the temperature was maintained at the hold temperature for the remainder of the experiment. Figure 2 shows a typical thermocouple trace for the thermocouples on the heated base plate and along the sides of the can. Experiments were conducted for the two hold temperatures and various orientations of the assembly relative to gravity.

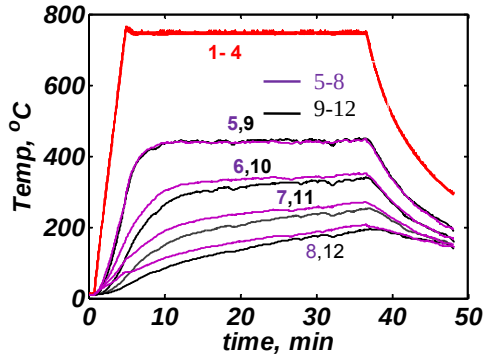

Figure 2. Thermocouple data used to specify boundary condition.

Experimental Test Matrix

The experimental test suite investigated the effect of orientation and hold temperature. Sixteen tests were conducted. Initially, twelve tests were conducted, a full-factorial design for two levels of temperature and three levels of orientation with replication. Units, initially reserved to address any failure during the first twelve tests, were then used to expand replication of 750 °C/upright 750 °C/side orientations, which were configurations anticipated to have (and which showed) the largest variability. The final combinations of hold temperature and orientation included

- 750 °C with 4 upright, 4 side, and 2 inverted
- 900 °C with 2 upright, 2 side, and 2 inverted.

For these tests, the as-cured foam mass varied from 0.165 to 0.188 g/cc. Samples with nominally the same density were chosen for a specific test configuration (hold temperature and orientation) Erickson et al. (2009).

NUMERICAL MODELING

The mathematical equations used to model the validation experiments include thermal conduction, chemical kinetics, and enclosure radiation. In addition, to approximate the thermal decomposition of the foam, individual elements are removed from the computation when the chemistry suggested that they had completely decomposed; this process is called "element death," Bova et al. (2006). Energy transport within the resulting void is assumed to be dominated by enclosure radiation through a non-participating media. Convection and foam liquifaction and flow are both neglected in this model.

Heat Conduction

The heat conduction within the foam, can, and component is given by

$$\rho C_p \frac{\partial T}{\partial t} - \nabla(k\nabla T) = Q_c \qquad (1)$$

where T is temperature, k is the thermal conductivity, ρ is the density, C_p is the specific heat, and *t* is time. The volumetric energy term Q_c accounts for the energy associated with chemical kinetics of the decomposing foam. The energy due to radiation transport is coupled to thermal conduction through (flux) boundary conditions. Separate, coupled mathematical equations describe chemical kinetics and radiation transport.

Chemical Kinetics (foam chemistry)

A general description of chemical kinetics used in the foam decomposition model is given next. In addition to the chemical kinetics, the REF chemistry model involves a vapor liquid equilibrium model, and lattice statistics. The details of the REF chemistry model are described in Hobbs (2003, 2005). Only equations for the chemical kinetics are discussed here.

A set of equations describe the allowable chemical reactions for *J* reactions and *I* species

$$\sum_{i=1}^{I} \nu'_{ij} M_i \rightarrow \sum_{i}^{I} \nu''_{ij} M_i \quad j = 1,\ldots,J \qquad (2)$$

In Eq. (2) ν''_{ij}, ν'_{ij} are stoichiometric coefficients and M_i is the chemical symbol for species *i*. Each reaction proceeds at a rate given by

$$r_j = k_j(T)\prod_i [N_i]^{\mu_{ij}} \quad j = 1,\ldots,J \qquad (3)$$

where N_i is the concentration of species *i* and μ_{ij} is the concentration exponent. The kinetic coefficient is expressed in Arrhenius form as

$$k_j = A_j \exp\left(\frac{-E_j + \sigma_{E_j}}{RT}\right) \qquad (4)$$

where A_j is the pre-exponential factor, E_j is the activation energy, T is the temperature, R is the universal gas constant, and σ_{E_i} is an activation energy distribution

factor. The rate of change in concentration for each species is written as

$$\frac{d}{dt}[N_i] = \sum_i (\nu''_{ij} - \nu'_{ij}) r_j \quad i = 1, ..., I \tag{5}$$

The chemical reaction process is coupled to thermal conduction through a volumetric energy term

$$Q_c = \sum_j r_j q_j \tag{6}$$

where q_j is the energy change due to reaction j , Hobbs, (2003).

In addition to the uncertainty associated with model input parameters, another uncertainty was included for the chemical decomposition model. Thermal decomposition was experimentally shown to depend on whether the decomposition products remain local to the decomposing foam, Erickson, et al. (2009). When decomposition products were "confined," i.e., not freely vented from the decomposing material, a difference in the mass loss curves was observed.

The chemistry model includes a dependence on confinement through a sub-grid model with a "confinement" parameter, Hobbs (2003). However, identifying a representative value for the confinement parameter, which was based on the small foam samples in thermogravimetric analysis (TGA) experiments, for the physical scenario for FIC was difficult. To address this situation, bounds on the confinement parameter were studied. The bounds of the confinement parameter span from "unconfined" chemistry to "partially confined" chemistry. To select the partially confined setting for the FIC conditions, the ratio of the venting area for the decomposing gasses to the surface area of the decomposing foam was used. The confinement parameter magnitude for the TGA experiments with the same ratio as the FIC assembly was used as the "partially confined" setting. Another approach would be to look at the resistance to diffusion as discussed in Hobbs (2005).

Thermal Decomposition of Foam ("element death")

The foam decomposes when heated, undergoing chemical kinetics that result in the (solid) structure transitioning to various gas, liquid, and solid decomposition products, Hobbs (2003). A simple approach to modeling this complex physical process is to assume that when a foam element has sufficiently decomposed it can be removed from the problem. The resulting void that evolves is assumed to be transparent and radiation exchange between the surfaces of the dynamically evolving enclosure is included. This procedure is implemented in a finite element code by removing elements representing foam material from the thermal conduction equations once the solid mass-fraction computed from the chemical kinetics is below a specified lower-threshold value. This process is called "element death" and is an approximate engineering model intended to account for material decomposition in a thermal conduction code based on the chemical state of the foam material and to account for thermal radiation in the resulting void.

Enclosure Radiation

Exchange of energy by radiation between *N* surfaces defining a transparent enclosure is described by

$$\sum_{j=1}^{N} \left[\frac{\delta_{kj}}{\varepsilon_j} - F_{k-j} \left(\frac{1-\varepsilon_j}{\varepsilon_j} \right) \right] \frac{Q_j}{A_j} = \sum_{j=1}^{N} \left(\delta_{kj} - F_{k-j} \right) \sigma T_j^4 \tag{7}$$

where ε_j is the surface emissivity, F_{i-j} is the view factor, Q_j is the net radiative energy, A_j is the surface area, σ is the Stefan-Boltzmann constant, and T is the surface temperature. These equations couple the radiative heat transfer to thermal conduction through the net flux on a surface. Using surface temperature from the conduction solution, net surface fluxes are computed and applied as boundary conditions to the surfaces of the enclosure.

COMPARISON OF PREDICTIONS AND TEST DATA

In comparing the model predictions and the measured temperature response, it is important to recognize two primary modeling assumptions and simplifications. First, the tests were conducted with the FIC unit in three different orientations which affect the foam response during decomposition. The numerical model has no dependence on orientation of the test device because it neglects convection and flowing liquids. Consequently, the model cannot be expected to predict or resolve any dependence on orientation. Secondly, no mass transfer of foam products of combustion is explicitly considered in the model. The effects of mass transfer on the chemical reaction rates were determined through TGA experiments and are included in the model using the "confinement" parameter previously discussed. The effect of this simplifying modeling approach is evaluated by varying this parameter as part of comparing model predictions and measured data.

Two metrics are used in comparisons of the numerical model and the measured data: a "temperature response" comparison (temperature as a function of time) and a "time to temperature rise" comparison (time for a specific increase). The "time to temperature rise" is the primary focus of this work due to the specific application of interest. Detailed comparisons, which include uncertainty quantification, will focus on this metric. Solution verification to assure these results are converged is discussed later in this paper.

Temperature Response Comparison

The measured temperature responses at TC 18 are compared to the model predictions for both partially-confined and unconfined chemistry in Figure 3. In this figure, a single model prediction for the multiple experiments of the same configuration is presented. Differences between the model predictions of multiple experiments were shown to be small in Dowding et al. (2005). These differences include variations in the initial bulk density of the foam and variations in the measured temperatures used as boundary conditions on the heated plate and along the sides of the FIC. Typical temperature responses for the TCs used as boundary

conditions are presented in Figure 2. The variations in average temperature of the heated plate are discussed in detail by Dowding et al. (2005)

The model predictions using the partially confined chemistry model responded more slowly than the response measured in the experiments. The predictions using the unconfined chemistry model responded more rapidly than the response measured in the experiments. For these predictions (both chemistry models), nominal values were used for all the other parameters. Consequently, the model predictions at the limits of unconfined and partially-confined chemistry parameter basically bound the experimental data. This indicates that the model is sensitive to the selection of the confinement parameter which is related to the mass transfer of decomposition products within the gas phase.

In some configurations, the temperature response of the model surpasses the temperature response of the experiment late in time. For the unconfined chemistry, there is also a different shape to the measured and predicted response curves. In particular, the measured temperature responses are concave downward, while the predicted temperatures are concave upward. These differences may be a result of modeling assumptions or relevant physics missing in the model.

Time to Temperature Rise Comparison

The time to temperature rise comparison, including model uncertainty and experimental measurements, is presented in Figure 4 for both the partially-confined and unconfined chemical models. For comparing time to temperature rise, model uncertainty due to input uncertainty (parameters and boundary conditions) was estimated. The process for propagating uncertainties through the model is discussed later in this paper. An uncertainty range defined by two standard deviations about the model prediction of time to temperature is shown in Figure 4. The mean measurement of time to temperature and a range defined by two standard deviations, both estimated from the multiple experiments (2 or 4) for a configuration, are also shown in Figure 4. The standard deviation in the time to temperature, not the average of time to temperature, is shown. Also shown is the measured time to temperature for each experiment (x-symbol). In general, the experimental uncertainty/variability for the 750 °C hold temperature was greater than for 900 °C.

For the partially-confined chemistry model, the comparison of time to temperature rise, including the effect of model uncertainty and measurement variability, indicated, for the most part, that the effects of uncertainty/variability would not account for the observed differences between the model predictions and experimental data. The exception to this conclusion was seen for the 5 °C temperature rise, where all configurations were within uncertainty and variability estimates. Predicting the early time response of the component indicated the model accurately represented conduction through the foam. At the low temperature rise, the model indicated that little of the foam had been decomposed.

The 750 °C configurations (Figure 4, a-c) have some orientations for which the differences fall within the uncertainty/variability estimates at the higher temperature rises (50, 100, and 150 °C). This was mainly for upright and side orientations, which showed large experimental variability (25% to 30%). For the experiment configurations at 900 °C (Figure 4, d-f), differences between the experimental measurements and model predictions with partially-confined chemistry were not explainable by uncertainty/variability estimates at the higher temperature rises (50, 100, and 150 °C).

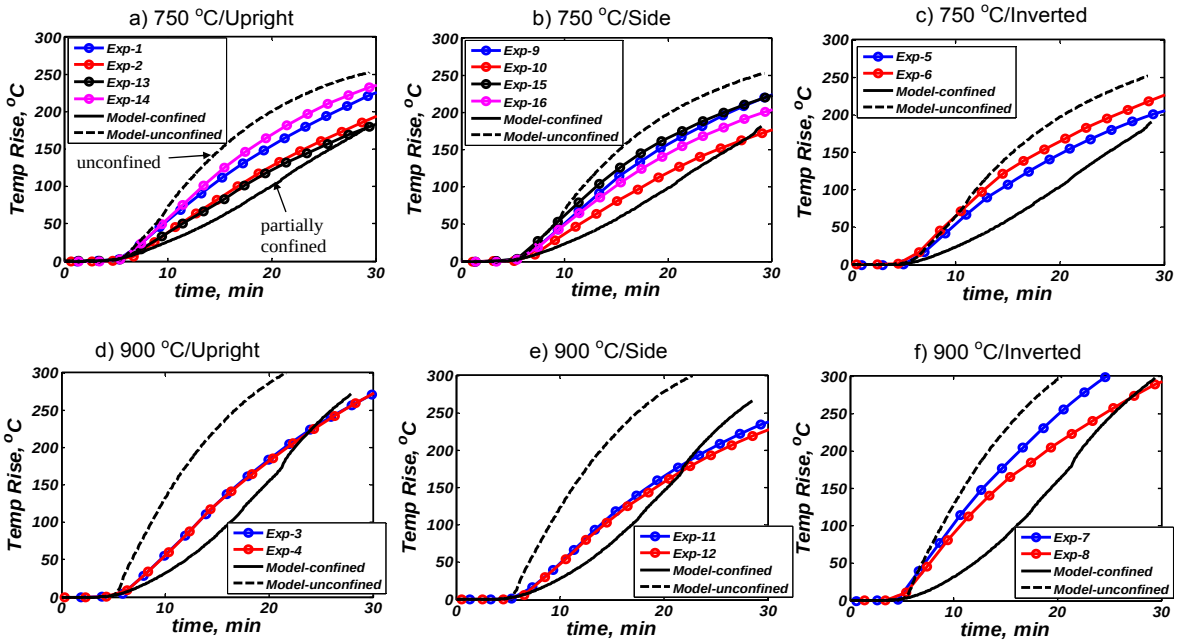

Figure 3. Measurement-prediction comparison using the unconfined and partially-confined chemistry models

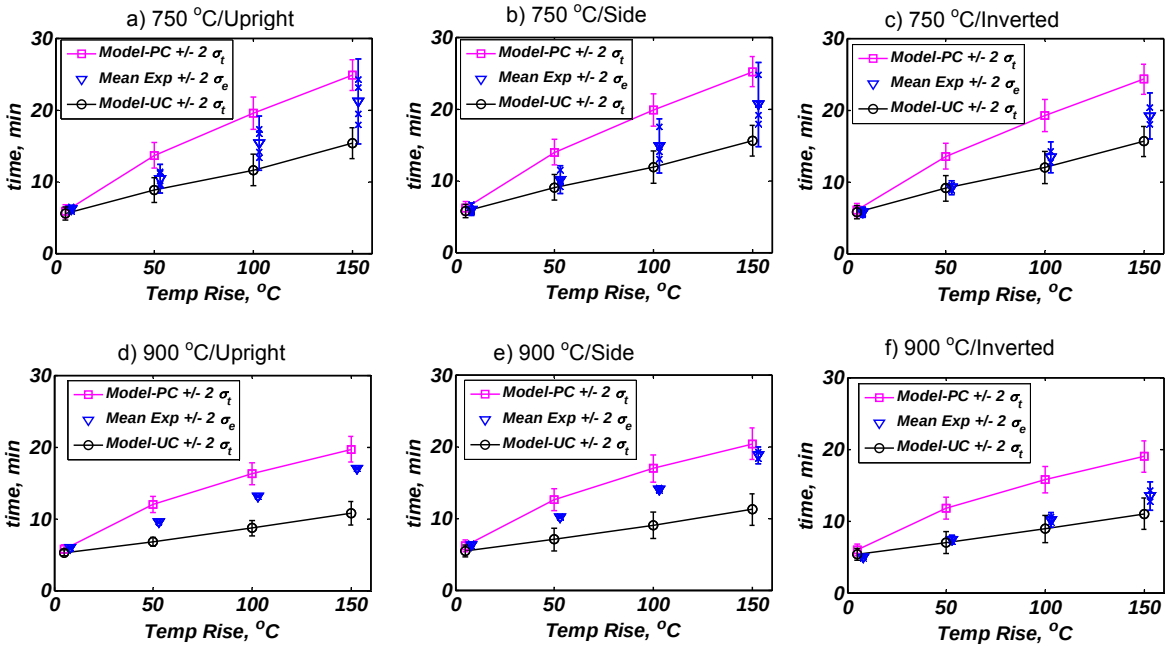

Figure 4. Measurement-prediction comparison of time to temperature for the unconfined and partially-confined chemistry model. The mean (over all experiments) of the model prediction is plotted with a model uncertainty range ($2\sigma_t$). The mean experimental measurement (triangle-symbol) is plotted with a two σ_e, where σ_e is the standard deviation among the experiments. Individual measurements are shown with the x-symbol.

For the unconfined chemistry model, the model predictions are predominantly below the experimental data (faster times to temperature). These model predictions were insensitive to confinement at the 5 °C temperature rise; differences between measurement and predictions were within estimates of uncertainty and variability. Differences at the higher temperature rises (50, 100, and 150 °C) were outside of estimates of uncertainty for several configurations.

For the 750 °C configurations (Figure 4, a-c), the differences between experimental data and model predictions may be explainable by uncertainty/variability estimates. For the experiment configurations at 900 °C (Figure 4, d-f), differences between the experimental measurements and model predictions with unconfined chemistry were not explainable by uncertainty/variability estimates at the higher temperature rises (50, 100, and 150 °C) with upright and side orientations. For the inverted orientation, the differences fall within the uncertainty/variability estimates for all temperature rises.

Model Uncertainty

The model uncertainty shown in Figure 5 was estimated by propagating uncertainty in the model parameters and boundary conditions through the model for both confinement parameters. Uncertainty in parameters associated with thermophysical properties of stainless steel and REF (foam), boundary conditions, and the REF decomposition chemistry model were analyzed.

Stainless steel thermophysical properties were from handbook values. The properties were piecewise-linear functions of temperature. Thermophysical properties of REF were also piecewise-linear functions of temperature. Experiments were conducted prior to the onset of decomposition (less than 100°C) to get low-temperature property values for REF. Properties at higher temperatures for REF were hypothesized based on expected behavior of the polymer properties, Hobbs (2003). Emissivity values for the heated plate were based on estimates/measurements for the Pyromark paint used to coat the surfaces. REF emissivity was based on estimates provided in Hobbs (2003). Parameters associated with the chemistry model, activation energies, distribution parameters on the activation energies, enthalpy of reaction, and element death criterion were taken from the chemistry model developed by Hobbs (2003). The temperature of the heated plate was used as the boundary condition and measured in the experiments.

The nominal estimates (mean) and standard deviations for all uncertain parameters are listed in Table **1**. The names listed in the first column identify the parameter and material/surface/location associated with the parameter. The naming convention for the parameters is thermal conductivity (k), specific heat (cp), emissivity (emis), temperature (temp), density (den), enthalpy of reaction (hr), chemistry solid fraction for element removal (death), activation energy (Ej), and activation energy distribution (sigEj). Following the parameter name is a material/surface/location modifier, stainless steel (ss), heated plate (BC-temp), and REF foam (ref). The model was evaluated using two bounding values for the confinement parameter because the appropriate confinement parameter is unknown for the FIC configuration. Model uncertainty was evaluated by

propagating the uncertainty in the other model parameters for both values of the confinement parameter.

A mean value approach was used to propagate parameter uncertainty through the model. The approach required gradients of the time to temperature with respect to the uncertain parameters. Gradients were approximated using central differences

$$\frac{\partial t(x)}{\partial p_i} \approx \frac{t(x, p_i + \delta p_i) - t(x, p_i - \delta p_i)}{2\delta p_i} \quad (8)$$

where t is the response (time to temperature), x is the location (of TC in mock component), and δp_i is the perturbation in the parameter. A 5% relative perturbation was used to approximate the gradients. Ideally, the perturbation would be related to the standard deviation in each parameter to get a global sensitivity. Unfortunately, this option was not available in Dakota (Eldred et al. 2002) at the time the analysis was run so a fixed relative perturbation was used to approximate the gradients.

In a mean value method, the gradients are post-processed to estimate the standard deviation in the response (Hills and Trucano, 1999)

$$\sigma_r = \left[\sum_{i=1}^{n_p} \left(\sigma_{p_i} \frac{\partial r}{\partial p_i} \right)^2 \right]^{1/2} \quad (9)$$

Equation (9) assumes the model parameters in Table 1 are uncorrelated, a reasonable assumption for most parameters and also appropriate given the limited data available for correlated chemistry parameters. To include the effect of correlation, when such data exist, see (Hills and Trucano, 1999).

It is informative to understand the contribution of each parameter to the total variance. Squaring Eq. (9), the relationship for estimating the response standard deviation and dividing through by the total variance (left side) gives a typical term in the summation

$$\gamma_i^2 = \frac{1}{\sigma_r^2} \left(\sigma_{p_j} \frac{\partial r}{\partial p_i} \right)^2 \quad (10)$$

where γ_i^2 is called the importance factor for parameter i. It represents the contribution of parameter p_i to the total variance. Each importance factor represents the fraction that a parameter contributes to the total variance.

The sensitivity coefficients (scaled by the nominal parameter value) and importance factors for the 750 °C/ upright case (Exp 1) with partially-confined chemistry are shown in Figure 5. These model uncertainty data are representative of all orientations because the model does not account for the effect of orientation. Other than minor differences between the foam bulk density and measured boundary temperatures, the other 750 °C experiments would show the same sensitivity and importance factors. The prediction of time to temperature is most sensitive to the boundary temperature (BC-temp). Other sensitivities are smaller and include the specific heat of the stainless steel (cp-ss), REF thermal conductivity (k-ref) and density (den-ref) of REF, and activation energy in the chemical kinetics decomposition model (E3).

Table 1. Uncertainty estimates of material properties and boundary conditions used to compute model uncertainty.

Parameter	Nominal	Relative Std Dev (%)	Source
k-ss	Function	10	Judgment
cp-ss	Function	5	Judgment
emis-ss	0.86	10	Pyrometer/Exp
BC-temp	Function	1	T/C error/Bias
den-ref (g/cc)	0.128	10	Hobbs*
k-ref	Function	10	Judgment
cp-ref	Function	10	Judgment
emis-ref	0.8	10	Judgment
hr-ref	Function	5	Hobbs* – TGA
death	0.162	5	Judgment
E1 (cal/mol)	28700	2.65	Hobbs* – TGA
E2 (cal/mol)	46400	2.33	Hobbs* – TGA
E3 (cal/mol)	58100	0.88	Hobbs* – TGA
E4 (cal/mol)	43500	4.40	Hobbs* – TGA
sigE1 (cal/mol)	760	39	Hobbs* – TGA
sigE2 (cal/mol)	2800	15	Hobbs* – TGA
sigE3 (cal/mol)	660	14	Hobbs* – TGA
sigE4 (cal/mol)	790	127	Hobbs* – TGA

* Hobbs (2003)

To focus the uncertainty/sensitivity analysis on the more significant parameters, only parameters that have the four largest importance factors or sensitivity coefficients are presented. However, because the parameters that comprise the largest magnitudes can vary with temperature rise (or time), some of these plots show more than four parameters to represent the top four contributors for all the temperature rises. The total uncertainty, "total var", represents the sum of the four largest importance factors; which in many cases, represents 90-95% of the total uncertainty.

The importance factors in Figure 5 indicate that 60-80% of the total uncertainty is due to thermal conductivity of the REF (k-ref). The remaining uncertainty is due to the specific heat of the stainless steel (cp-ss), density of REF (den-ref), heated plate temperature (BC-temp), solid fraction criterion for element death (death), and thermal conductivity of stainless steel (k-ss). For the 900 °C/upright configuration, the parameters with the largest sensitivity coefficients are similar to the previous 750 °C case. Overall, the model is less sensitive to parameters (smaller magnitude of scaled sensitivity coefficients) at the 900 °C hold temperature than at the 750 °C hold temperature (Dowding et al. 2005).

The uncertainty analysis for the unconfined chemistry setting shows the same group of parameters with the largest sensitivities as was observed for the partially-confined chemistry. Consequently, it can be concluded that the main contributors to the total uncertainty were also not sensitive to confinement. The total uncertainty using unconfined chemistry had a large contribution from thermal conductivity of REF, with the same group of parameters accounting for the remaining uncertainty.

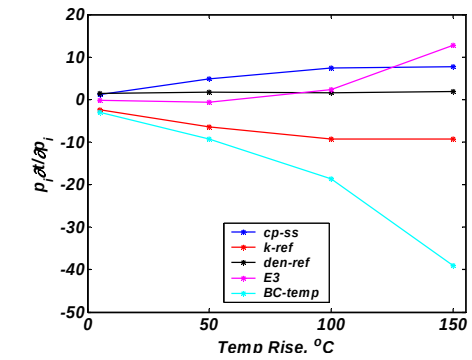

a) Scaled Sensitivity Coefficients

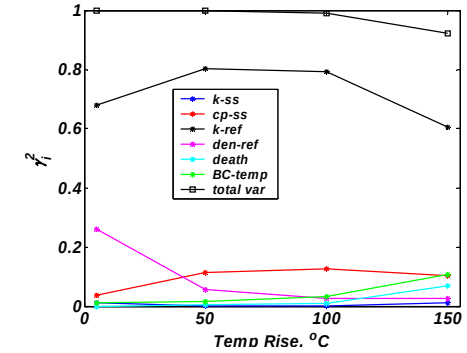

b) Importance Factors

Figure 5. Scaled sensitivity coefficients and importance factors for 750 °C/upright prediction.

A Latin hypercube sampling (LHS) approach was also used to estimate the model uncertainty. Only slight differences in the estimated uncertainty (mean and standard deviation) were observed between the LHS and mean value. The ranking of the important parameters was consistent for the LHS and mean value method. The consistency between the LHS and mean value method suggests that the model is closely approximated as a linear function of the parameters (Dowding et al. 2005).

Solution Convergence

To assess the dependence of the predicted solution to the mesh discretization parameters and solution timestep size, a sequence of solutions with varying timesteps (Δt) and different characteristic element sizes (*h*) was considered. Because the uncertainty quantification calculations require many simulations, it is extremely important that the numerical model be as computationally efficient as possible, within acceptable bounds of discretization error. Mesh discretization effects must also be sufficiently small so that there is no possibility of masking the effects of different physics and configurations. The following analyses assess the solution sensitivity to the element size and evaluate the solution accuracy in the context of other uncertainty and variability considerations. Based on these analyses, an acceptable mesh (characteristic element edge length) for use in these comparisons was established.

Table 2 summarizes the combinations of timestep and element size studied, as well as the other computational considerations (number of cpus and computer run times). Note that the finer meshes not only have smaller elements, but they also required smaller timesteps for the comparison of the solution sensitivity to mesh discretization. The timestep was selected to maintain a constant ratio of timestep over characteristic element size squared ($\Delta t/h^2$). Note that the computational effort for solutions using the medium mesh (~6x the number of elements in the coarser mesh) was typically 34-55 times the effort required for the coarser mesh.

Table 2. Summary of mesh and timesteps considered to evaluation solution sensitivity to numerical parameters

Elem size "h" (cm)	Timestep (Δt) (sec)	$\Delta t/h^2$	Elems (K)	Nodes (K)	CPUs	Time (cpu-hrs)
0.6	4	11.11	3.4	4	4	1
0.6	2	5.56	3.4	4	4	1.2
0.6	1	2.78	3.4	4	4	1.8
0.6	0.5	1.39	3.4	4	4	2.7
0.3	1.0	11.11	20	22	32	34
0.3	0.5	5.56	20	22	32	62
0.3	0.25	2.78	20	22	32	100
0.3	0.125	1.39	20	22	32	150
0.15	0.5	22.22	151	160	48	500

To understand the significance of the sensitivity of the computed solution to mesh discretization, results were compared with the variability in the experimental data. Figure 6 shows this comparison for the 900 °C/inverted configuration, which was the configuration with smallest experimental variability. The figure shows that solution differences due to mesh effects are negligible (approximately an order of magnitude smaller) in comparison to both experimental variability and solution uncertainty. The coarse mesh (*h* = 0.6) and the auto timestep feature were used throughout this work.

The time to temperature for solutions using the three meshes as a function of timestep (actually $\Delta t/h^2$) for the 50 and 150 °C temperature rises was computed for TC 18 using the partially-confined chemistry model. The time to temperature rise was insensitive to the magnitude of the time step for a given mesh size. The difference between a mesh size of 0.6 and 0.3 is approximately 0.1 min, which is 0.8% and 0.5% of the time to a 50 and 150 °C temperature rise, respectively. This result is an upper bound on the difference because all simulations done in this project utilized the automatic timestep option, which will further reduce the difference.

SUMMARY AND CONCLUSIONS

The model predictions and data agreed best for the early time response of the component. The agreement of the model at later time (high temperature rises) was poorer. Late time behavior should be dominated by getting the correct quantity of net energy to the component. The poor agreement at later time would indicate the component was getting less energy in the

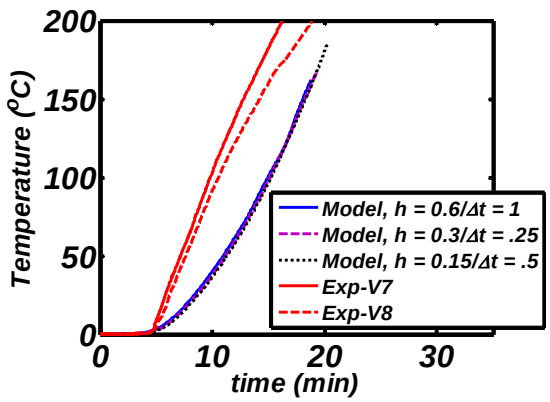

Figure 6. Comparison of measured temperature response for the 900 °C/inverted case to model predictions at three levels of mesh density.

experiment than the model (with partially-confined chemistry) would predict. The shape of the measured and predicted thermal response curves (Figure 6) was different with partially confined chemistry, but more similar with unconfined chemistry. The thermal response of the model with unconfined chemistry appears more representative of the experimental response, but responds too quickly.

The experiments at 750 °C indicated far greater experimental variability than that explained by parameter variability in the model. This may indicate that the model for parameter variability (uncertainty) underestimated the actual variability. Another possible explanation is that the variability is caused by effects (physics) that are not included in the model. For example, foam liquifaction, natural convection, and participating media radiation in the evolving enclosure were not included in the model. The 900 °C configurations did not exhibit large experimental variability.

The modeling approach used element death to remove foam from the thermal model when the chemistry model indicated the foam had completed decomposition (reached a critical mass fraction). The foam was removed on an element-basis from the finite element model. When the foam had completed decomposition, the elements originally containing foam were modeled as transparent voids with enclosure radiation across them. This approximation (foam elements decomposing and opening voids) presumes the decomposing foam leaves no structure or material behind.

Postmortem observation by opening the FIC assemblies showed that material was present in the region between the heated plate and component (Erickson et al. 2009). Sufficient material remained to obscure visibility of the component. Whether the material was present during the experiment or formed afterwards is not known. If material was present during the experiment, it would act as a radiation shield and inhibit energy transfer to the component, and may explain the discrepancy in the model. We believe this behavior may be important and research is under way to develop models that account for the effect of material remaining after the foam decomposes.

The FIC assemblies were designed as a severe and focused test of decomposition chemistry model and heat transfer modeling of the thermal response of components embedded in foam. The intended application will have other contributing heat transfer modes and may be less sensitive to the presence of foam, and to the accuracy of the thermal decomposition model. To describe the accuracy of the model in future applications, uncertainty bounds defined by a partially-confined and unconfined chemistry model will be used (bounds the experimental data). While these uncertainty bounds are quite large, because this was a severe test of the foam thermal-decomposition model, other applications will include other uncertain parameters and may be less sensitive to the present foam decomposition model.

REFERENCES

Bova, S. W., Copps, K. D., and, Newman, C. K. (2006) "Calore, A Computational Heat Transfer Program, Volume 1: Theory Manual," SAND2006-6083P, Sandia National Laboratories, Albuquerque, NM.

Dowding, K. J., Hogan, R. E., Erickson, K. L., Trujillo, S. M., and Hobbs, M. L. (2009) " Validation Assessment for Modeling the Thermal Response of Components Embedded in Removable Epoxy Foam – Experimental Data and Analysis," 20th International Symposium on Transport Phenomena, 7-11 July, 2009, Victoria, BC, Canada.

Dowding, K. J., Hogan, R. E., Hobbs, M. L., Erickson, K. L., and Trujillo, S. M. (2005) "Validation Assessment for Modeling the Thermal Response of Components Embedded in Removable Epoxy Foam," SAND2005-5754, Sandia National Laboratories, Albuquerque, NM.

Eldred, M. S., Giunta, A. A., van Bloemen Waanders, B. G., Wojtkiewicz, S. F., Hart, W. E., and Alleva, M. P. (2002) "DAKOTA, A Multilevel Parallel Object-Oriented Framework for Design Optimization, Parameter Estimation, Uncertainty Quantification, and Sensitivity Analysis, Version 3.0 Users Manual," SAND2001-3796, Sandia National Laboratories, Albuquerque, NM.

Erickson, K. L., Trujillo, S. M., Oelfke, J. B., Hanks, C. R., Belone, B., and Ramirez, D. M. (2009) "Component-Scale Removable Epoxy Foam (REF) Thermal Decomposition Experiments ("MFER" series, April 2003) Supporting the FY04/Q2 Level 1 V&V Milestone. Part 1: Temperature Data," SAND Report in draft. Sandia National Laboratories, Albuquerque, NM.

Hills, R. G. and Trucano, T. G. (1999) "Statistical Validation of Engineering and Scientific Models: Background," SAND1999-1256, Sandia National Laboratories, Albuquerque, NM.

Hobbs, M. L. (2003) "SREF – A Simple Removable Epoxy Foam Decomposition Chemistry Model," SAND2003-4550, Sandia National Laboratories, Albuquerque, NM.

Hobbs, M. L. (2005) "Modeling epoxy foams exposed to fire-like heat fluxes," *Polymer Degradation and Stability*, Vol. 89, pp. 353-372.